AD 262 335

DISCLAIMER NOTICE

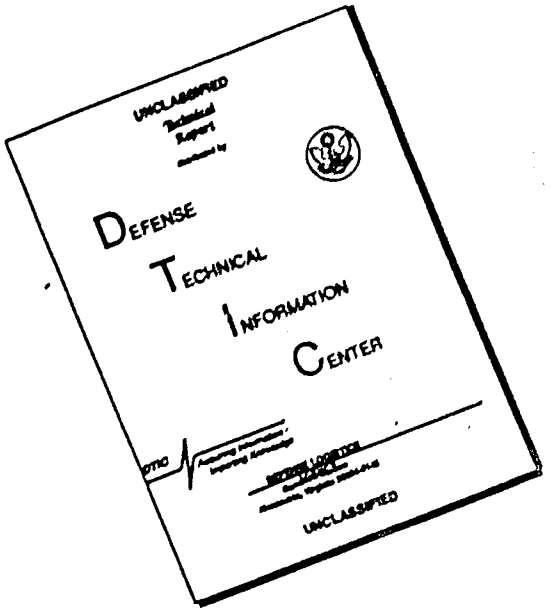

THIS DOCUMENT IS BEST QUALITY AVAILABLE. THE COPY FURNISHED TO DTIC CONTAINED A SIGNIFICANT NUMBER OF PAGES WHICH DO NOT REPRODUCE LEGIBLY.

PRINCETON UNIVERSITY

DEPARTMENT OF AERONAUTICAL ENGINEERING

NATIONAL AERONAUTICS
AND SPACE ADMINISTRATION

NASA Grant NsG-99-60

NONLINEAR ASPECTS OF COMBUSTION INSTABILITY IN LIQUID PROPELLANT ROCKET MOTORS

First Yearly Progress Report
For the Period 15 June 1960 to 31 May 1961

Aeronautical Engineering Report No. 553

Prepared by: David T. Harrje
D. T. Harrje, Research Engineer

Assisted by: W. A. Sirignano
W..A. Sirignano, Asst-in-Research

and David M Ashford
D. M. Ashford, Asst-in-Research

Approved by: Luigi Crocco
L. Crocco, Professor-in-Charge

1 June 1961

Department of Aeronautical Engineering
PRINCETON UNIVERSITY
Princeton, New Jersey

TABLE OF CONTENTS

I. INTRODUCTION

Research under NASA Grant NsG-99-60 was undertaken as a part of the Jet Propulsion Research Program of the Department of Aeronautical Engineering at Princeton to "conduct an experimental-theoretical study of nonlinear effects in combustion instability in liquid rocket motors. This basic study would also investigate the causes and magnitudes of the nonlinear perturbations, which are of special concern in the design of high thrust rocket systems."

II. SUMMARY

An optical model of a no-flow rocket motor has been completely designed and is currently in an early phase of testing. The object of this optical rocket motor is threefold: (1) to establish the characteristics of the incoming perturbation - in the current system a perturbation produced by a pulse generator utilizing blank cartridges and precision diaphragms, (2) to aid in evaluating the velocity probe prior to its insertion into a "hot" rocket motor, and (3) to observe, for the applied perturbation, the shock wave patterns produced and the time for decay under varying rocket motor conditions.

Preliminary results have already yielded important data on items (1) and (3) and under item (2) the probe is being modified for considerably smaller target areas because of the shock wave strengths encountered. The shape of the wave as well as its strength will improve the basic understanding of the problem and hence influence the inputs into the theoretical model calculations.

Nonlinear rocket tests so far have consisted of rechecking one chamber-injector combination to determine the stability limits prior to the

introduction of nonlinear perturbations. Actual perturbation tests will begin within the next few weeks.

A solution to the theoretical model based on strong shock waves rotating in the chamber is being attempted using IBM 650 equipment. A number of improvements and simplifications have been made in the program but as yet no solution has been found.

III. DISCUSSION

In this first year of operation, the effort in the "Nonlinear Aspects of Combustion Instability in Liquid Propellant Rocket Motors" research sponsored by NASA has concentrated on three areas: (1) The optical model of the combustion chamber, (2) the design of hardware and initiation of tests on the nonlinear rocket motor and (3) the solution of the first theoretical model relating to nonlinear considerations. The status of these three items will be covered in this report.

A. Optical Model of the Rocket Motor

The optical model of the combustion chamber has been evolved with a number of objectives in mind. In order to study the effects of nonlinearities in any system, one must first be able to measure the perturbation introduced. In previous approaches to the problem only empirical relationships were sought. The onset of nonlinear instability was measured in terms of number of powder grains in an explosive charge (Ref. 1) or number of psi in an entering stream of high velocity gas (Ref. 2). The first portion of this research therefore is concerned with evaluating exactly what takes place at the station where the propellants are injected, since it is there that early events in the combustion process take place.

The experimental approach to evaluating such effects within the chamber is based first on simulating the geometry of the rocket chamber cross

section (under no through flow conditions). Using optical techniques, velocity probes, and transient pressure instrumentation, the time history of the transverse flow conditions due to the entering shock pulse are being recorded. Figures 1 and 2 illustrate this experimental apparatus located in the newly completed laboratory room addition to the nonlinear combustion instability rocket cell.

The object of this optical rocket model is threefold: (1) to establish the characteristics of the incoming perturbation - in the current system a perturbation produced by a pulse generator utilizing blank cartridges and precision diaphragms, (2) to aid in evaluating the velocity probe prior to its insertion into a "hot" rocket motor, and (3) to observe, for the applied perturbation, the shock wave patterns produced and the time for decay under varying rocket motor conditions.

Concerning the experimental apparatus itself, the schematic of Figure 2 is most helpful in the overall operation of the system. Basically, a two-pass schlieren or shadowgraph system is used. A spark is fired shortly after a shock pulse enters the chamber with a photograph taken of the resulting density gradients. Details of the individual items of apparatus are as follows.

The optical rocket motor is identical to the operating rocket hardware as far as the cylindrical portion of the combustion chamber is concerned. In both cases, the cylindrical section is four inches long and is composed of two individual chamber sections, one containing the pulse gun locations (See Figure 3). Each chamber section provides for three pressure transducers located at 90° intervals. The sections may be turned with respect to each other to provide pressure instrumentation at intervals less than 90°. This will be important in the identification of the higher modes of oscillation. Although it is felt that the

tangential pulse gun location (Figure 3) will receive the bulk of experimental attention, a radial pulse location has also been supplied.

The injection end plate in the optical rocket motor is designed to provide for the velocity probes at the same locations as in the "hot" injector (Figure 4). Ten locations are provided. In the case of the optical injection end plate, the major consideration is the optical quality of the plate. Manufactured from a stainless steel plate with velocity probe plugs, the face was ground to an accuracy of $\pm$ 2 wave lengths of sodium light. Testing to date has caused only barely detectable errosion on the injector plate from flying bits of diaphragm from the shots fired. Tarnishing and smoke deposits are removed after each tests using alcohol applied with cotton wadding. In the absence of a shock pulse small surface irregularities from the grinding process are visible on the injector face. However as can be seen in Figure 5 (which describes an early test on the optical model and will be described later in more detail), the shock pulse and associated turbulence make such irregularities unimportant in the interpretation of the optical data. Therefore, grinding to 1/4" wave length or adding a nickel coating to improve reflectivity and protect the surface do not appear necessary at this time.

At the other end of the chamber, rather than the convergent portion of the nozzle, there is instead an optically flat glass plate. In order to meet the requirement of chamber pressures as high as 1,000 psi with a nine inch chamber diameter, the design is based on 1-1/4 inch thick glass (the thickest in normal production). For the higher pressures tempered glass will be used (tempered glass has poorer optical qualities but four times higher strength), while at the lower pressures the polished plate glass with an ultimate strength which allows a 500 psi (max.) chamber pressure is desirable. The method of clamping should provide an additional safety factor of 1.C. All testing is done remotely, in any

case, due to the uncertainness in the glass strengths.

The pulse gun is a modified version of the type used by Aerojet in combustion instability tests. The principle is based on the use of a carefully sized charge of rapidly burning gunpowder to burst a precision manufactured diaphragm. Thus a controlled perturbation is supplied to the rocket motor being tested. The pulse gun is shown in Figure 3 and consists of a modified Mauser bolt action assembly to position and fire the blank cartridge. The solenoid trips the conventional trigger mechanism which in turn signals the spark system via the microswitch located on the rear of the bolt action. Internally, as is shown in Figure 6, the firing pin activates the primer, the flash of which ignites the charge of pistol powder causing the buildup of pressure behind the diaphragm which bursts at a controlled pressure level. Within the cartridge, a metal spacer has been added to keep the dead space between cartridge and diaphragm constant. Three grain charges are currently anticipated - 45, 30 and 15 grains. In the present tests, only the 15 grain charges have been used with the 7500 psi diaphragm.

Returning to the schematic of Figure 2, the next item is the 10 inch, 80 inch focal length, optically ground mirror ($\pm$ 1/4 wave length).

After the mirror along the optical path, is the initial light source, the knife edge and the photographic equipment. Light is supplied from a spark which discharges in a period of 1 millionth of a second (sufficiently fast to reduce possible blurring to an acceptable level) with energy supplied from a discharging 15KV, .5μf condenser. The spark source (borrowed from the Gas Dynamics Group) is quite simple and dependable. Initially, the optical system with the knife edge is lined up using a steady source of light from a zirconium arc lamp. The timing of the spark is of particular importance since the shock waves degenerate in the

order of a few milliseconds. Therefore, an electronic timing circuit activated by the previously mentioned micro switch provides the appropriate time prior to spark discharge. A multiple-spark firing system, where a series of charged condensers are discharged in turn across the spark gap will be utilized shortly in the test apparatus. Based on an automotive distributor principle, where rotational speed will determine time intervals, problems center about maintaining a small tickle charge so that at either the distributor points or the spark gap no problem of a nonionized condition exists and thus restricts discharge.

The flash of the pulse gun itself has been shown to be important as a source of light, with intensities of the same order as that of the spark. Since the shutter must be opened in the darkened test room awaiting the spark, filters limiting light to the ultra violet range were used in addition to increasing the spark intensity to reduce flash interference.

Currently, the photographic equipment is quite simple and consists of a remotely operated shutter on a portrait camera where the image has been prefocused on ground glass. The camera is off to side due to space requirements and hence a flat mirror is used (See Figure 1). Since with a two-pass schlieren system, alignment must include an angular deviation in the overall optical path, a number of images are produced. At the knife edge, the brightest image is selected and the remainder are masked out. When the multiple spark system is used, the photographic complexities will increase accordingly. Since requirements are such that six photographs must be taken in an approximately three millisecond interval, a drum camera is called for. A 6 inch diameter drum camera is available and will require rotational speeds of 12,000 RPM to separate the photographs using 16MM film. Blurring during the period of the spark would be limited to approximately .001 inch and would be quite acceptable.

The instrumentation used in these tests, other than the optical system, has already been mentioned briefly, namely, the pressure transducers and the velocity probes. The latter require additional explanation, however, since they must still be considered in the development stage. Figure 7 gives a cross-sectional representation of the velocity probe. An extremely simple device, it is shown to consist of the sensing target, the pressure seal, ball linkage, strain gage column, second pressure seal and electrical connections. The strain gages are supplied with either 3 or 6 volt DC and provide a 1 millivolt signal (with 3 volts) for 10 pound load on the target. One important area of development has been in the case of the targets, where a material capable of withstanding rocket temperature (5000^{o}F+), and high heat transfer rates (15 BTU/in^{2}/sec or more are present with strong transverse combustion instability) was sought. Various materials were tested in motors operating on the "linear" program and included lucite, graphite, ceramic coated stainless steel, ceramic coated copper, boron nitride, astrolite and other glass reinforced composition, and GRB silicon carbide. The only materials which withstood the conditions (from minus several hundred degrees to operation for two seconds at approximately 5000^{o}F) were the GRB silicon carbide and the ceramic coated copper and in the latter case, a new ceramic coat was necessary for each test. More recent tests of the GRB silicon carbide target are shown in Figure 8, which illustrates how well this material stands up under the high heat flux rates as well. These tests were run on the square motor in the "linear" program (Reference 3).

Sizing of the targets is under further consideration. Testing in the optical rocket motor has shown the size to be too large for close proximity to the incoming pulse (the darkened spot in Figure 5 indicates this position). Plastic and aluminum targets were damaged in the early

tests indicating forces well beyond preliminary estimates. More recently a hollow stainless steel rod was used with no damage resulting. Until a fuller knowledge of the shock wave pattern is obtained, a probe cannot be calibrated in the optical apparatus directly. However, with the correct target shape known calibration will take place in available shock tubes.

Since the optical rocket has only been in operation over the past few weeks, any data must be considered preliminary. The photograph shown in Figure 5 illustrates one type of data that is being sought with this apparatus. The curved shock pattern when compared to the point where the shock pulse is introduced would indicate that although the pulse is oriented tangentially, the shock initially travels across the chamber. The point of injection is seen to be displaced from the center of the resultant spherical wave. However, port shape, wall reflections and the variation in gas properties due to the incoming shock pulse could account for this. Schlieren photos at various points during the shock growth should help answer such questions.

Pressure and velocity probe data from these tests have been found to add additional information as to the sequence of events following the first pressure rise (which is difficult to observe due to resonance in the transducers in the presence of a step function input). The pressure records indicate that at least by the third distinct pulse, pressure pulsations are traveling tangentially in the direction of the pulse gun orientation.

B. The Nonlinear Rocket Motor

Based on the wide variety of tests performed on the "linear" combustion instability program, it was decided to use an injector-chamber

combination that had already exhibited a clear set of combustion stability limits when mixture ratio was varied. The combination chosen was the 500 pound thrust level, 1.4 design mixture ratio spuds using an eight inch injection diameter in a nine inch diameter chamber.

The planning behind the testing on this rocket motor is shown in the schematic of Figure 9. Starting from a known set of stability limits for the standard rocket conditions (only combustion noise present and starting transients guarded against with destructable barriers, Ref. 4) the perturbation level will be raised in a controlled fashion and any shift in stability limits will be noted. The perturbation will be supplied from the pulse guns tested on the optical rocket motor. It is hoped that a relationship between the deviation of the stability limits can be correlated with the basic parameters associated with the rocket motor design.

Currently the standard conditions are being rechecked, since the velocity of any comparisons rests on these standard limits. This same injector type has also been involved in recent tests with the "linear" program. Certain starting difficulties, which have resulted in the loss of rocket hardware (Ref. 3), have limited the number of tests on the nonlinear hardware until the difficulty could be cleared up. New starting procedures and safety instrumentation are now incorporated in the test operation of both researches and testing will increase rapidly in the next few weeks. Since this test stand is closely tied to the results and checkout of instrumentation on the optical rocket motor, testing on both stands must proceed in a coordinated fashion.

Ceriain other nonlinear data which is constantly being collected as a by-product of the "linear" program will also be checked out in far greater detail on the nonlinear rocket motor.

C. The Nonlinear Theoretical Model

A complete description of the nonlinear theoretical model is covered in Appendix A with the detailed equations stated in Appendix B.

From the theoretical point of view, a knowledge of velocity and pressure perturbations is important in the determination of inputs into the numerical solutions currently in progress. Briefly, the theoretical attack to date has involved a model consisting of a cylindrical annular-type chamber with a constant flow of premixed gases entering at one end. The resulting theory would also be applicable in a conventional cylindrical chamber near the wall.

In the model pressure disturbances rotate in the transverse direction with constant velocity and constant wave length. All combustion is assumed to occur when the premixed gas is swept by the disturbance the first time, thus a generalized Chapman-Jouget detonation criterion applies. The release of energy in combustion is considered the driving mechanism for the system.

From these and other considerations the four basic algebraic equations have been derived. They involve (1) the Chapman-Jouget condition, (2) the Hugoniot relation, (3) the isoenergetic, and (4) isentropic relations applied between the disturbances. Since all pressure waves are assumed to be purely transverse, the axial velocity is constant throughout the flow and the axial momentum equation is trivial. Important factors in these conservation equations are the lengths of the detonation region and the shock region of the disturbance. They appear as weighting factors in the equations.

Acquisition (on a rental basis) of an IBM 1620 computer late this summer will greatly alleviate the major problem in the solution of the theoretical model so far, that of having adequate machine time. Recent

breakdowns and the heavy load of other University research have limited access to the 650 machine to only a few hours per week.

Solution of the first theoretical model will be followed by the more complex case where the curvature of the shock waves is taken into consideration.

APPENDIX A

Theoretical Model of Nonlinear Combustion Instability

For initial simplicity in determining a theoretical model for the phenomenon of nonlinear combustion instability, a cylindrical annular-type combustion chamber has been considered with a constant flow of premixed gases entering at one end. The resulting theoretical treatment may also be applied near the wall of a conventional cylindrical chamber.

In the model, one or more pressure disturbances (assumed concentrated in an axial plane) rotate in a transverse direction with constant velocity and constant wave length. Each disturbance is identical in nature and extends the length of the chamber. All the combustion occurs when the premixed gas is swept by the disturbance for the first time. In the following sweeps, no combustion occurs, just non-isentropic compression. Therefore, the portion of the disturbance near the injector is a detonation (assumed to be the Chapman-Jouget type since this is the only stable type one can imagine). The other portion of the disturbance is a pure shock wave. In between these concentrated compression waves, expansion waves exist and these must move in a transverse direction, also.

The release of energy in combustion is considered the driving mechanism for the system.

If the reference frame is fixed to this disturbance, the problem becomes a two-dimensional steady type, and independent variables are the axial and transverse coordinates. Radii are assumed large enough to neglect centrifugal effects and radial variations in fluid properties are neglected. In the formulation of the theory, average values are used for the velocities, pressures and densities at the surface of the concentrated disturbances. Averages over each of three regions are used. These

regions are: the region of unburned gases at the upstream surface of the detonation, the region of burned gases at the upstream surface of the shock, and the region of burned gases at the downstream surface of the concentrated disturbance.(See Figure 10).

The assumption is made that the average pressures are the same for the burned and unburned regions at the upstream surface of the disturbance. All coefficients of non-uniformity which would appear in this formulation are assumed to be unity.

The conservation equations for mass, energy, and the transverse component of momentum are applied across the surface of the disturbance as a whole. Since all pressure waves are purely transverse, the axial velocity is constant throughout the flow and the axial momentum equation adds no additional information. Important parameters appearing in these conservation equations are the lengths of the detonation region and the shock region of the disturbance. They appear as weighting factors in the equations. These lengths must be determined as functions of the pressures, densities, and velocities at the surfaces of the disturbance and at the injector surface. This is accomplished by means of an investigation of the particle trajectory in the unburned gas region.

The assumption is made that the pressure gradient in the transverse direction is constant near the injector. The isentropic condition is applied throughout the unburned gas region, and allows a determination of the functional dependence of these lengths upon certain pressures, densities, and velocities.

The application of the isoenergetic condition in this region of unburned gases adds a new unknown, the velocity of the disturbance relative to the chamber. This is also the transverse velocity component (in the frame of reference) of the gas at the injector surface. The isoenergetic

condition may be applied at the end of the analysis to determine the velocity of the disturbance.

The isentropic and isoenergetic conditions are applied across the region of expanding burned gases to relate average fluid properties at the downstream surface of one disturbance to properties at the shock portion of the upstream surface of the next disturbance. These relations actually connect properties on one side of the disturbance to properties on the other side because of the cyclic nature of the model.

The Chapman-Jouget condition is applied across the detonation. That is, the velocity of propagation of the detonation wave is minimized with respect to the pressure ratio across the disturbance. Note that the thermodynamic properties in front of the detonation are considered constant in the differentiation. It must be noticed, however, that this particular way of applying the Chapman-Jouget condition contains a certain element of arbitrariness.

The following parameters are assumed to be known initially: quantity of heat released in combustion, specific heat ratio (assumed the same everywhere), chamber length, wave length of disturbance, average thermodynamic properties of premixed gases at injection, and the axial velocity component of premixed gases at injection. The unknowns are the average values for the pressures, densities, and transverse velocities along the disturbance and, also, the propagation velocity of the disturbance relative to the chamber. There are now equal numbers of unknowns and equations.

For the equations themselves, the following nomenclature will be used:

a = speed of sound

p = pressure

ρ = density

u = velocity

λ = wave length

L = chamber length

ℓ' = length of detonation portion of disturbance

k' = length of shock portion of disturbance

γ = ratio of specific heats

V_s = velocity of disturbance relative to chamber

V_I = longitudinal velocity of gas throughout the field

q = energy per unit mass of reactant released in combustion

Subscripts

$1u$ = conditions at unburned region at upstream surface of disturbance

$1b$ = conditions at burned region at upstream surface of disturbance

2 = conditions at downstream surface of disturbance

i = conditions at surface of injector

It is convenient to nondimensionalize as follows:

$$\varphi = p_2/p_1 \qquad Q = q/a_i^2$$

$$\Theta = \rho_2/\rho_{1u} \qquad \lambda = \lambda'/L$$

$$\Psi = \rho_{1b}/\rho_{1u} \qquad \ell = \ell'/L$$

$$Z = u_{1u}^2/a_i^2 \qquad k = k'/L$$

The isentropic condition is applied along a streamline in the unburned gas region to obtain the following relation between conditions at the injector and at the surface of the disturbance $\rho_{1u} = \rho_i \left(\frac{2}{1+\varphi}\right)^{1/\gamma}$. The length of the detonation zone ℓ is easily found as a function of

ϕ and z by relating the mass flow through the injector to the mass flow through the detonation region. Thus,

$$\ell = \frac{\lambda \frac{V_1}{a_i}}{\sqrt{z}} \left(\frac{1+\varphi}{2} \right)^{1/\gamma}$$

so that,

$$k = 1 - \ell = 1 - \frac{\lambda \frac{V_1}{a_i}}{\sqrt{z}} \left(\frac{1+\varphi}{2} \right)^{1/\gamma}$$

The three conservation equations may be applied across the disturbance. Mass and momentum equations are used to eliminate u_1 and u_2 from the conservation of energy equation. This results in an equation of the form

$$F\left(\varphi, \theta, z, \psi, Q, \lambda \frac{V_1}{a_i}, \gamma\right) = 0 \qquad (1)$$

The isoenergetic condition applied in the region of burned gases gives another relation between properties at the surfaces of the disturbances. Again, the equations of the conservation of mass and momentum are used to eliminate velocities. The relation is of the form

$$G(\varphi, \theta, \psi, z, \gamma) = 0 \qquad (2)$$

The isentropic condition applied in the region of burned gases provides still another relation,

$$\theta/\psi = \varphi^{1/\gamma} \qquad (3)$$

This equation is used to eliminate ψ from Equations (1) and (2) to obtain

$$F(\varphi, \theta, z, Q, \lambda \frac{V_1}{a_i}, \gamma) = 0 \qquad (4)$$

and

$$G(\varphi, \theta, z, \gamma) = 0 \qquad (5)$$

The Chapman-Jouget condition indicates that

$$\left.\frac{\partial u_{1a}}{\partial \varphi}\right|_{\frac{P_i}{P_{1a}}=\text{Const.}} = 0 \quad \text{or} \quad \left.\frac{\partial z}{\partial \varphi}\right|_{\frac{P_i}{P_{1a}}=\text{Const}}$$

which is equivalent to

$$H(\varphi, \theta, z, Q, \lambda \tfrac{V_I}{a_i}, \gamma) = \left.\frac{\partial F}{\partial \varphi}\right|_{P/P_{1a}} \cdot \left.\frac{\partial G}{\partial \theta}\right|_{P/P_{1a}} - \left.\frac{\partial F}{\partial \theta}\right|_{P/P_{1a}} \cdot \left.\frac{\partial G}{\partial \varphi}\right|_{P/P_{1a}} = 0 \quad (6)$$

Equations (4), (5) and (6) are three simultaneous equations in the variables φ, θ, and z and the parameters Q, $\lambda \frac{V_I}{a_i}$, and γ. The problem is then one of solving these three equations for the values of φ, θ, and z for given values of Q, $\lambda \frac{V_I}{a_i}$, and γ. The three equations are given in full form in Appendix B.

This theoretical problem is in the process of being solved using an IBM 650 computer. An iteration scheme is being used.. Rather than arbitrarily choosing starting values for φ, θ, and z in the iteration scheme, the IBM 650 is calculating the values of the functions $F(\varphi, \theta, z)$ and $H(\varphi, \theta, z)$ at each of a lattice of points in φ, θ, z space. From this plot of points a rough estimate of the geometry of the $F = 0$, $G = 0$, and $H = 0$ surfaces may be expected. At this time, the values of F, G, and H have been determined at a lattice of points covering the space $1 \leq \varphi \leq 25$, $1 \leq \theta \leq 25$, and $1 \leq z \leq 25$ for the cases of $Q = 50$ and 100, with $\gamma = 1.25$ and $\lambda \frac{V_I}{a_i} = 0.1$. A more complete coverage of possible values of Q and $\lambda \frac{V_I}{a_i}$ are planned in the near future. Realistic values of γ cover a small range so that 1.25 is taken as representative. These represent the physical limits of the parameters and any meaningful solution should be within these limits.

In the results to date for each of the two cases discussed above, the line of intersection of the $F = 0$ and the $G = 0$ surfaces did not intersect with the $H = 0$ surface. With the higher value of Q, the

surfaces are further from simultaneous solution. As yet, the effect of λ^{V_2}/a_i on the solution has not been observed. The possibility that a relaxation or modification of the Chapman-Jouget condition may be necessary in order to obtain a simultaneous solution is presently being investigated.

8

APPENDIX B

System of Equations and Variables

Variables $\varphi = P_2/p_1$

$\theta = \rho_2/\rho_{1u}$

$\psi = \rho_{1b}/\rho_{1u}$

$z = u_{1u}^2/a_i^2$

Equations (1) Hugoniot relation across disturbance

(2) Isoenergetic relation between disturbances

(3) Isentropic relation between disturbances

(6) Chapman-Jouget condition

These are easily reduced to three equations in three variables φ, θ, and z, by use of the isentropic relation to eliminate ψ. Equations (1), (2) and (3) are replaced by Equations (4) and (5) which have no dependence on ψ. The terms p_1 and ρ_{1u} will be related to φ and the injector conditions by the assumption $p_i = \frac{p_1 + p_2}{2}$ and by the isentropic relations applied in the unburned gas region. The system of equations becomes:

$$F(\varphi, \theta, z) = 0 \qquad (4)\text{-}1$$

$$G(\varphi, \theta, z) = 0 \qquad (5)\text{-}1$$

$$\left.\frac{\partial z}{\partial \varphi}\right|_{P_1/P_{1u}=\text{const}} = H(\varphi, \theta, z) = \left.\frac{\partial F}{\partial \theta}\right|_{P_i/\rho_{1u}} \left.\frac{\partial G}{\partial \varphi}\right|_{P_i/\rho_{1u}} - \left.\frac{\partial F}{\partial \varphi}\right|_{P_i/\rho_{1u}} \left.\frac{\partial G}{\partial \theta}\right|_{P_2/P_{1u}} = 0 \qquad (6)\text{-}1$$

These equations can be written out in terms of the following quantities:

$$\ell = \lambda \frac{V_I}{a_i} \frac{1}{\sqrt{z}} \left(\frac{1+\varphi}{2}\right)^{1/\gamma} \qquad \gamma, \lambda\frac{V_I}{a_i}, Q \text{ are constants}$$

$$K = 1 - \lambda \frac{V_I}{a_i} \frac{1}{\sqrt{z}} \left(\frac{1+\varphi}{2}\right)^{1/\gamma}$$

$$\sigma = \frac{1}{2}\left(\frac{\varphi^{1/\gamma}}{K} - 1\right)\left[1 - \frac{\theta}{\ell} + \frac{1}{\gamma}\frac{\theta(\varphi-1)}{z\ell^2}\left(\frac{2}{1+\varphi}\right)^{\frac{\gamma-1}{\gamma}}\right]$$

$$\frac{\partial\sigma}{\partial\theta} = \frac{1}{2}\left(\frac{\varphi^{1/\gamma}}{K} - 1\right)\left[\frac{1}{\gamma}\frac{(\varphi-1)}{z\ell^2}\left(\frac{2}{1+\varphi}\right)^{\frac{\gamma-1}{\gamma}} - \frac{1}{\ell}\right]$$

$$\frac{\partial\sigma}{\partial\varphi} = \frac{\varphi^{\frac{1-\gamma}{\gamma}}}{2\gamma K}\left[1 - \frac{\theta}{\ell} + \frac{1}{\gamma}\frac{\theta(\varphi-1)}{z\ell^2}\left(\frac{2}{1+\varphi}\right)^{\frac{\gamma-1}{\gamma}}\right] +$$

$$\left(\frac{\varphi^{1/\gamma}}{K} - 1\right)\frac{\theta}{2\gamma z\ell^2}\left(\frac{2}{1+\varphi}\right)^{\frac{\gamma-1}{\gamma}}$$

Thus,

$$F(\varphi,\theta,z) = 0 = \left(\frac{\varphi^{\frac{1}{\gamma}}}{K} - 1\right)\left\{\frac{1}{\gamma-1}\left(\frac{2}{1+\varphi}\right)^{\frac{\gamma-1}{\gamma}} + \frac{z}{2} + Q\right\}$$

$$+ \left(1 + \sqrt{1+2\sigma}\right)\left\{\frac{1}{\gamma-1}\left(\frac{2}{1+\varphi}\right)^{\frac{\gamma-1}{\gamma}}\frac{\varphi^{\frac{1}{\gamma}}}{\theta} + \left[\frac{z\ell^2}{\left(1-\frac{K}{\varphi^{1/\gamma}}\right)^2\theta^2}\right]\left[1 + \sigma + \sqrt{1+2\sigma}\right]\right\}$$

$$- \left(\frac{\varphi^{1/\gamma}}{K} + \sqrt{1+2\sigma}\right)\left\{\frac{1}{\gamma-1}\left(\frac{2}{1+\varphi}\right)^{\frac{\gamma-1}{\gamma}}\frac{\varphi}{\theta} + \left[\frac{z\ell^2}{2\left(1-\frac{K}{\varphi^{1/\gamma}}\right)^2\theta^2}\right]\left[1 + \frac{K}{\varphi^{1/\gamma}}\sqrt{1+2\sigma}\right]^2\right\} \quad (4\text{-}2)$$

$$G(\varphi,\theta,z) = 0 = \frac{2}{\gamma-1}\theta(\varphi - \varphi^{1/\gamma})\left(\frac{2}{1+\varphi}\right)^{\frac{\gamma-1}{\gamma}} \quad (5\text{-}2)$$

$$- \frac{z\ell^2}{(1-K/\varphi^{1/\gamma})}\left[\left(1 + \frac{K}{\varphi^{1/\gamma}}\right)(1+2\sigma) + 2\sqrt{1+2\sigma}\right]$$

The four factors in Equation (6-1) are the following:

$$\left.\frac{\partial F}{\partial \theta}\right|_{P_t/P_{1u}} = \left(\frac{\frac{\partial \sigma}{\partial \theta}}{\sqrt{1+2\sigma}}\right)\left\{\frac{1}{\gamma-1}\left(\frac{2}{1+\varphi}\right)^{\frac{\gamma-1}{\gamma}}\frac{\varphi^{\gamma}}{\theta} + \left[\frac{z\ell^2}{\left(1+\frac{k}{\varphi^{1/\gamma}}\right)^2\theta^2}\right]\left[1+\sigma+\sqrt{1+2\sigma}\right]\right\}$$

$$+\left(1+\sqrt{1+2\sigma}\right)\left\{-\frac{1}{\gamma-1}\left(\frac{2}{1+\varphi}\right)^{\frac{\gamma-1}{\gamma}}\frac{\varphi^{\gamma}}{\theta^2} + \left[\frac{z\ell^2}{\left(1-\frac{k}{\varphi^{1/\gamma}}\right)^2\theta^2}\right]\left[1+\sigma+\sqrt{1+2\sigma}\right]\right.$$

$$\left.-\left[\frac{2z\ell^2}{\left(1-\frac{k}{\varphi^{1/\gamma}}\right)^2\theta^3}\right]\left[1+\sigma+\sqrt{1+2\sigma}\right]\right\} - \left(\frac{\frac{\partial \sigma}{\partial \theta}}{\sqrt{1+2\sigma}}\right)\left\{\frac{1}{\gamma-1}\left(\frac{2}{1+\varphi}\right)^{\frac{\gamma-1}{\gamma}}\frac{\varphi}{\theta} + \right.$$

$$\left.+\left[\frac{z\ell^2}{2\left(1-\frac{k}{\varphi^{1/\gamma}}\right)^2\theta^3}\right]\left[1+\frac{k}{\varphi^{1/\gamma}}\sqrt{1+2\sigma}\right]^2\right\} - \left(\frac{\varphi^{\frac{1}{\gamma}}}{k}+\sqrt{1+2\sigma}\right)\left\{-\frac{1}{\gamma-1}\left(\frac{2}{1+\varphi}\right)^{\frac{\gamma-1}{\gamma}}\frac{\varphi}{\theta^2}\right.$$

$$\left.+\left[\frac{z\ell^2 k}{\left(1-\frac{k}{\varphi^{1/\gamma}}\right)^2\theta^2\varphi^{1/\gamma}}\right]\left[\left(1+\frac{k}{\varphi^{1/\gamma}}\sqrt{1+2\sigma}\right)\frac{\frac{\partial \sigma}{\partial \theta}}{\sqrt{1+2\sigma}}\right] - \left[\frac{z\ell^2}{\left(1-\frac{k}{\varphi^{1/\gamma}}\right)^2\theta^3}\right]\left[1+\frac{k}{\varphi^{1/\gamma}}\sqrt{1+2\sigma}\right]^2\right\}$$

$$\left.\frac{\partial G}{\partial \varphi}\right|_{P_t/P_{1u}} = \frac{2}{\gamma-1}\theta\left(1-\frac{1}{\gamma\varphi^{\frac{\gamma-1}{\gamma}}}\right)\left(\frac{2}{1+\varphi}\right)^{\frac{\gamma-1}{\gamma}} + \frac{z\ell^2 k}{\gamma\left(1-\frac{k}{\varphi^{1/\gamma}}\right)^2\varphi^{\frac{\gamma+1}{\gamma}}} \cdot$$

$$\cdot\left[\left(1+\frac{k}{\varphi^{1/\gamma}}\right)(1+2\sigma)+2\sqrt{1+2\sigma}\right] - \frac{z\ell^2}{\left(1-\frac{k}{\varphi^{1/\gamma}}\right)}\left[2\left(1+\frac{k}{\varphi^{1/\gamma}}+\frac{1}{\sqrt{1+2\sigma}}\right)\frac{\partial \sigma}{\partial \varphi}\right.$$

$$\left.-(1+2\sigma)\frac{k}{\gamma\varphi^{\frac{\gamma-1}{\gamma}}}\right]$$

$$\left.\frac{\partial G}{\partial \theta}\right|_{P_t/P_{1u}} = \frac{2}{\gamma-1}\left(\varphi-\varphi^{1/\gamma}\right)\left(\frac{2}{1+\varphi}\right)^{\frac{\gamma-1}{\gamma}}$$

$$-\frac{2z\ell^2}{\left(1-\frac{k}{\varphi^{1/\gamma}}\right)}\left[1+\frac{k}{\varphi^{1/\gamma}}+\frac{1}{\sqrt{1+2\sigma}}\right]\frac{\partial \sigma}{\partial \theta}$$

$$\frac{\partial F}{\partial \varphi}\Big|_{p/p_m} = \frac{\varphi^{\frac{1-\gamma}{\gamma}}}{\gamma k}\left\{\frac{1}{\gamma-1}\left(\frac{2}{1+\varphi}\right)^{\frac{\gamma-1}{\gamma}} + \frac{z}{2} + Q\right\} + \left(\frac{\frac{\partial\sigma}{\partial\varphi}}{\sqrt{1+2\sigma}}\right)\left\{\frac{1}{\gamma-1}\left(\frac{2}{1+\varphi}\right)^{\frac{\gamma-1}{\gamma}}\frac{\varphi^{1/\gamma}}{\theta} + \right.$$

$$\left. + \left[\frac{z\ell^2}{\left(1-\frac{k}{\varphi^{1/\gamma}}\right)^2\theta^2}\right]\left[1+\sigma+\sqrt{1+2\sigma}\right]\right\} + \left(1+\sqrt{1+2\sigma}\right)\left\{\frac{1}{\gamma(\gamma-1)}\left(\frac{2}{1+\varphi}\right)^{\frac{\gamma-1}{\gamma}}\frac{\varphi^{\frac{1-\gamma}{\gamma}}}{\theta} + \right.$$

$$\left. + \left[\frac{z\ell^2}{\left(1-\frac{k}{\varphi^{1/\gamma}}\right)^2\theta^2}\right]\left[\left(1+\frac{1}{\sqrt{1+2\sigma}}\right)\frac{\partial\sigma}{\partial\varphi}\right] - \left[\frac{2z\ell^2 k}{\gamma\left(1-k/\varphi^{1/\gamma}\right)^3\theta^2\varphi^{\frac{\gamma-1}{\gamma}}}\right]\cdot\right.$$

$$\left.\cdot\left[1+\sigma+\sqrt{1+2\sigma}\right]\right\} - \left(\frac{\varphi^{\frac{1-\gamma}{\gamma}}}{\gamma k} + \frac{\frac{\partial\sigma}{\partial\varphi}}{\sqrt{1+2\sigma}}\right)\left\{\frac{1}{\gamma-1}\left(\frac{2}{1+\varphi}\right)^{\frac{\gamma-1}{\gamma}}\frac{\varphi}{\theta} + \right.$$

$$\left. + \left[\frac{z\ell^2}{2\left(1-\frac{k}{\varphi^{1/\gamma}}\right)^2\theta^2}\right]\left[1+\frac{k}{\varphi^{1/\gamma}}\sqrt{1+2\sigma}\right]^2\right\} - \left(\frac{\varphi^{1/\gamma}}{k} + \sqrt{1+2\sigma}\right)\cdot$$

$$\cdot\left\{\frac{1}{\gamma-1}\left(\frac{2}{1+\varphi}\right)^{\frac{\gamma-1}{\gamma}}\frac{1}{\theta} + \left[\frac{z\ell^2}{\left(1-\frac{k}{\varphi^{1/\gamma}}\right)^2\theta^2}\right]\left[\left(1+\frac{k}{\varphi^{1/\gamma}}\sqrt{1+2\sigma}\right)\cdot\right.\right.$$

$$\left.\left.\cdot\left(\frac{k}{\varphi^{1/\gamma}}\frac{\frac{\partial\sigma}{\partial\varphi}}{\sqrt{1+2\sigma}} - \frac{k}{\gamma\varphi^{\frac{\gamma+1}{\gamma}}}\sqrt{1+2\sigma}\right)\right] - \left[\frac{z\ell^2 k}{\gamma\left(1-k/\varphi^{1/\gamma}\right)^3\theta^2\varphi^{\frac{\gamma+1}{\gamma}}}\right]\cdot\right.$$

$$\left.\cdot\left[1+\frac{k}{\varphi^{1/\gamma}}\sqrt{1+2\sigma}\right]^2\right\}$$

Using the solution for ϕ , θ , z , we find the following:

$$\psi = \frac{\theta}{\varphi^{1/\gamma}} \quad ; \quad V_{s/a_i} = \sqrt{z + \frac{2}{\gamma-1}\left[\left(\frac{2}{1+\varphi}\right)^{\frac{\gamma-1}{\gamma}} - 1\right]}$$

$$u_{1b/a_i} = \frac{\sqrt{z}\,\ell}{\theta\left(1-k/\varphi^{1/\gamma}\right)}\left[1+\sqrt{1+2\sigma}\right]$$

$$u_{1u/a_i} = \frac{\sqrt{z}\,\ell}{\theta\left(1-k/\varphi^{1/\gamma}\right)}\left[1+k/\varphi^{1/\gamma}\sqrt{1+2\sigma}\right]$$

REFERENCES

1. Ellis, H., "Liquid Propellant Rocket Combustion Research," Edwin G. Baetjer, II, Colloquium, Princeton University, Feb. 9, 1960.

2. Mower, W., Baker, D., and Jackson, E., "Application of Stability Rating Techniques to Large Thrust Chambers" (CONFIDENTIAL) ARS Meeting, Palm Beach, Apr. 26, 1961.

3. Harrje, D. T., and Reardon, F. H., "Combustion Instability In Liquid Propellant Rocket Motors," 35th Report for the Period 1 Nov. 1960 to 30 May 1961, Princeton University Aeronautical Engineering Report No. 216-11, 1 June 1961.

4. Harrje, D. T., Reardon, F. H., "Combustion Instability In Liquid Propellant Rocket Motors," 31st Quarterly Report for the Period 1 Nov. 1959 to 31 Jan. 1960, Princeton University Aeronautical Engineering Report No. 216-ee, 31 March 1960.

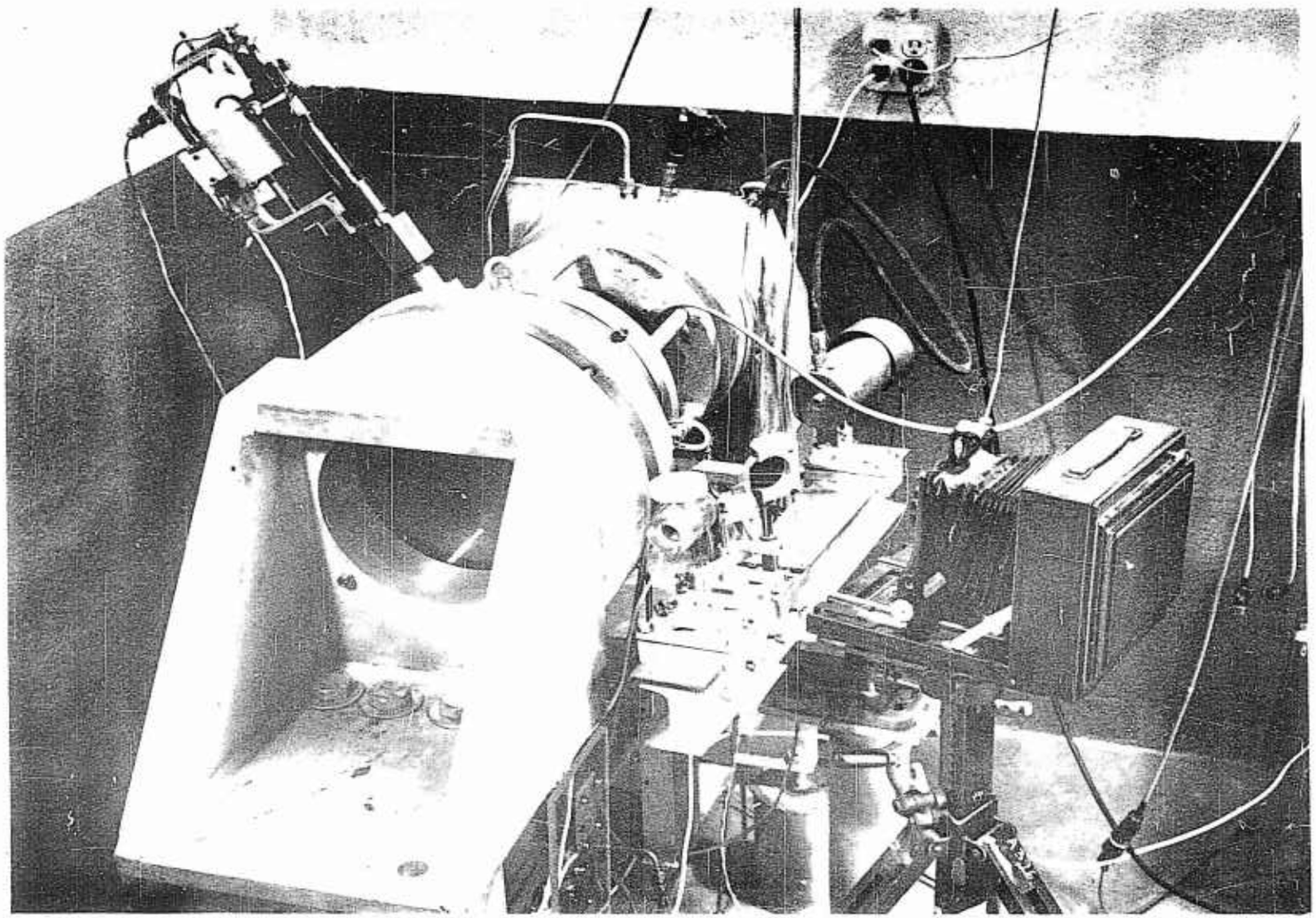

Nonlinear optical rocket motor,
spark source and camera

Figure 1

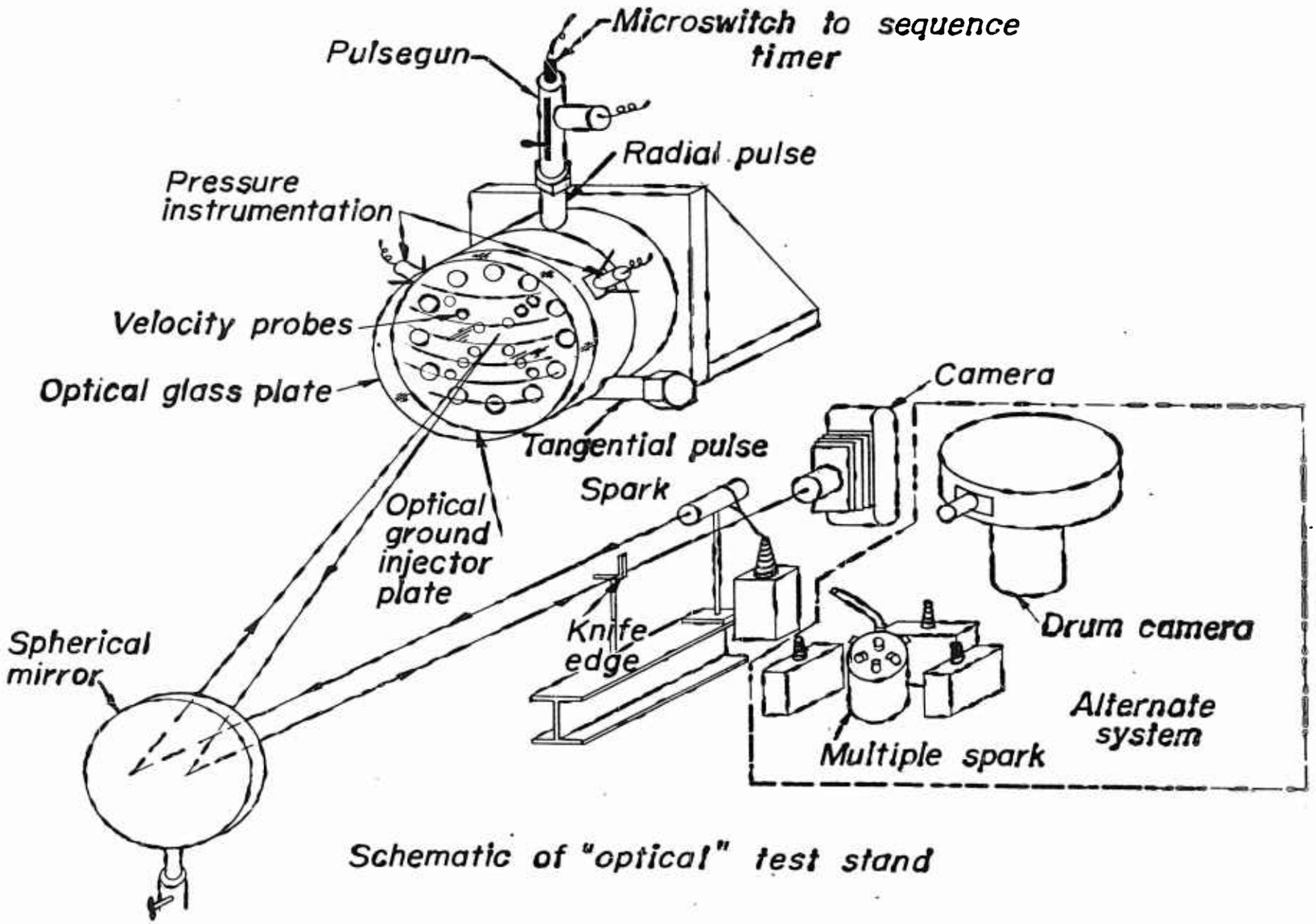

Schematic of "optical" test stand

Figure 2

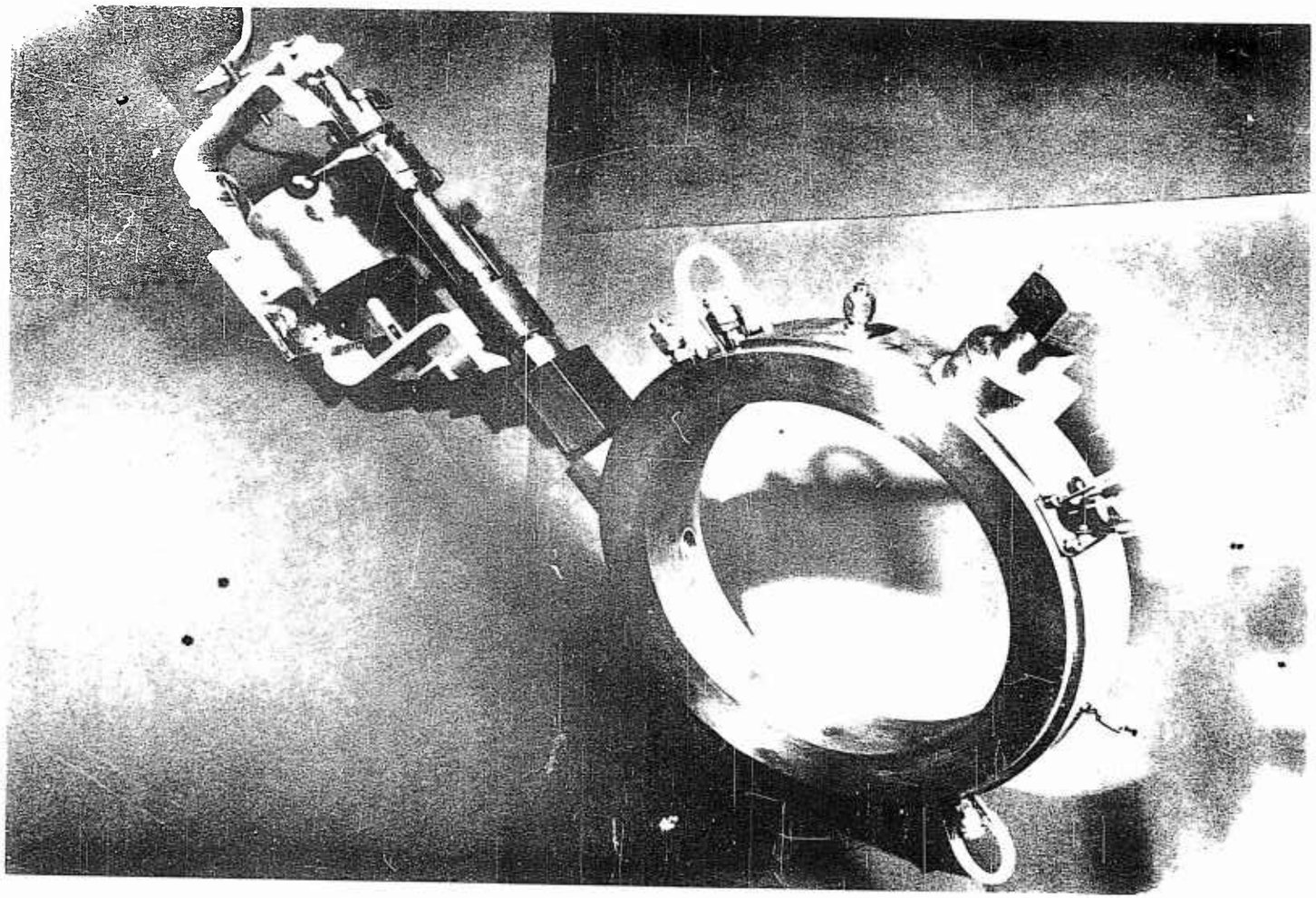

Figure 3

First chamber section with pulse gun in tangential firing position

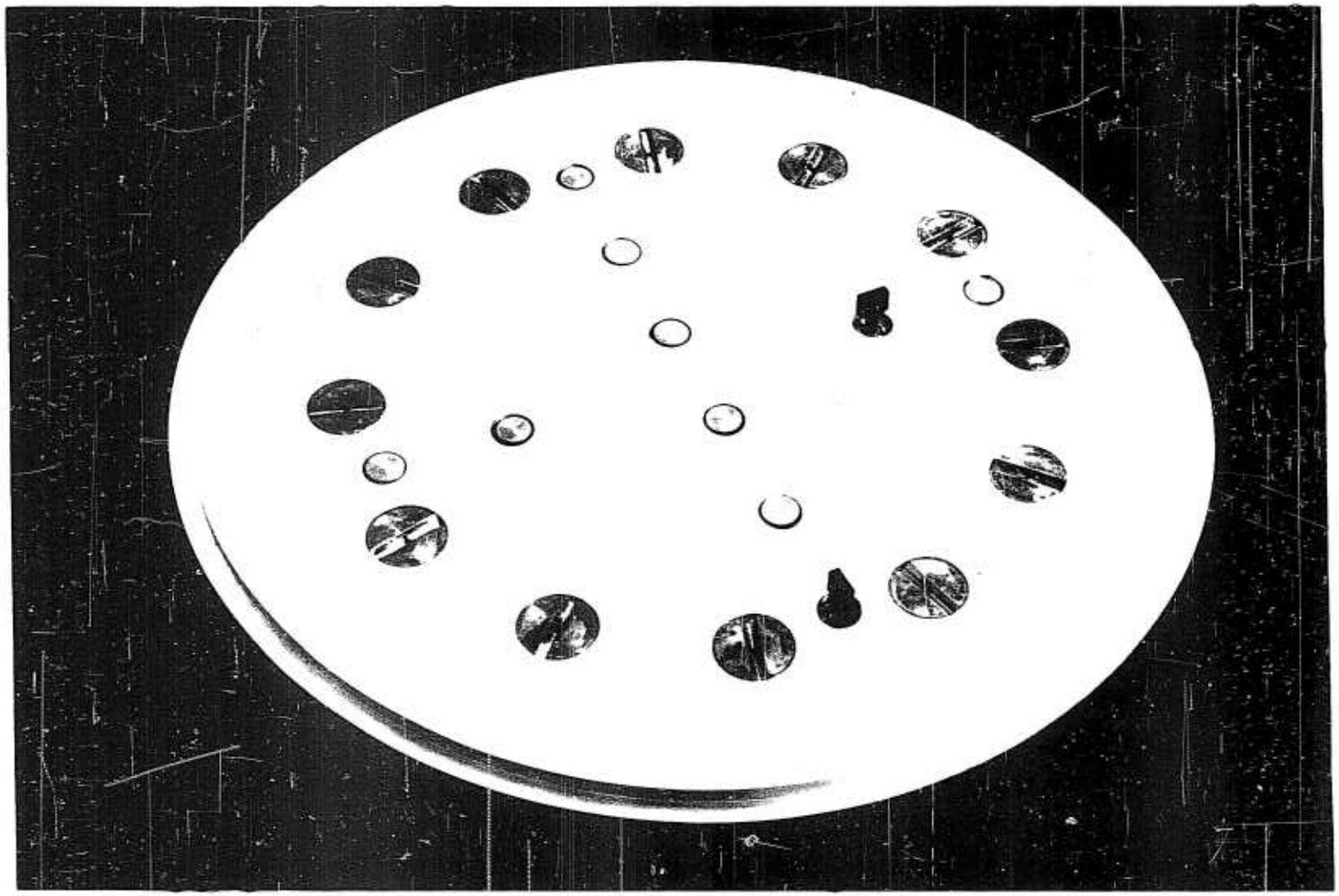

Figure 4

Injector plate with 2 velocity probes in place and tangential oriented spuds

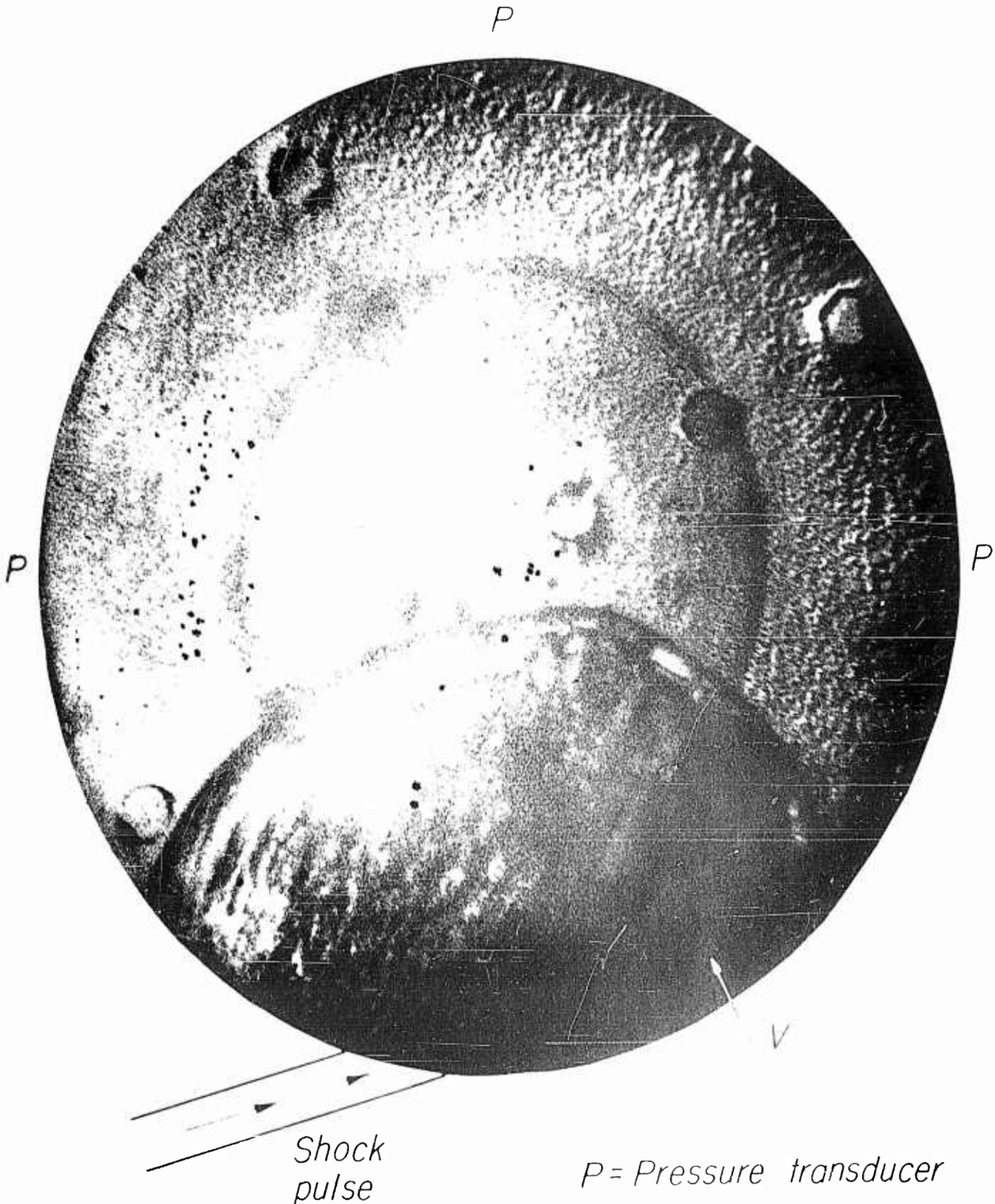

Early schlieren photograph of shock pulse

Figure 5

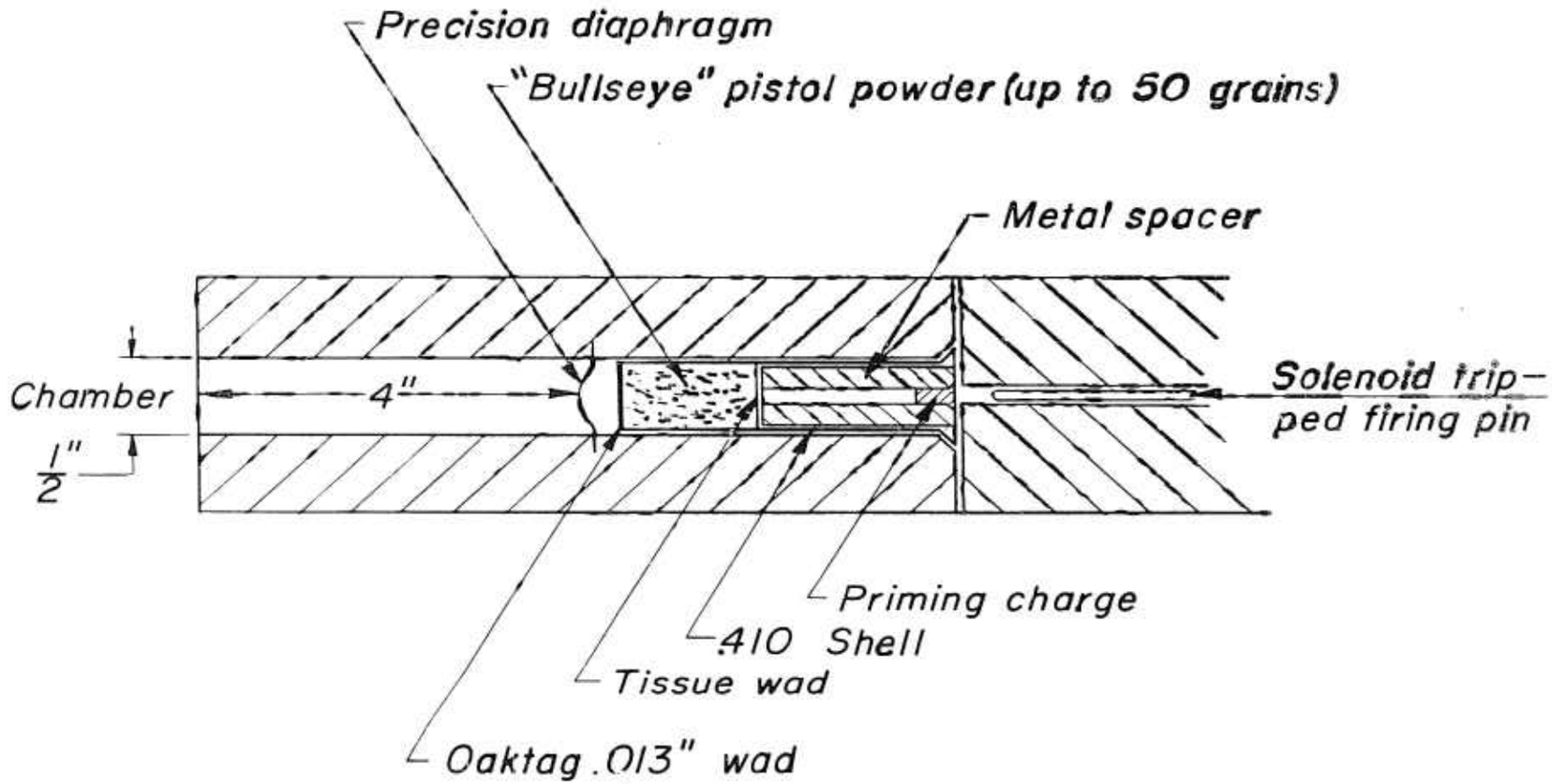

Pulse gun cutaway

Figure 6

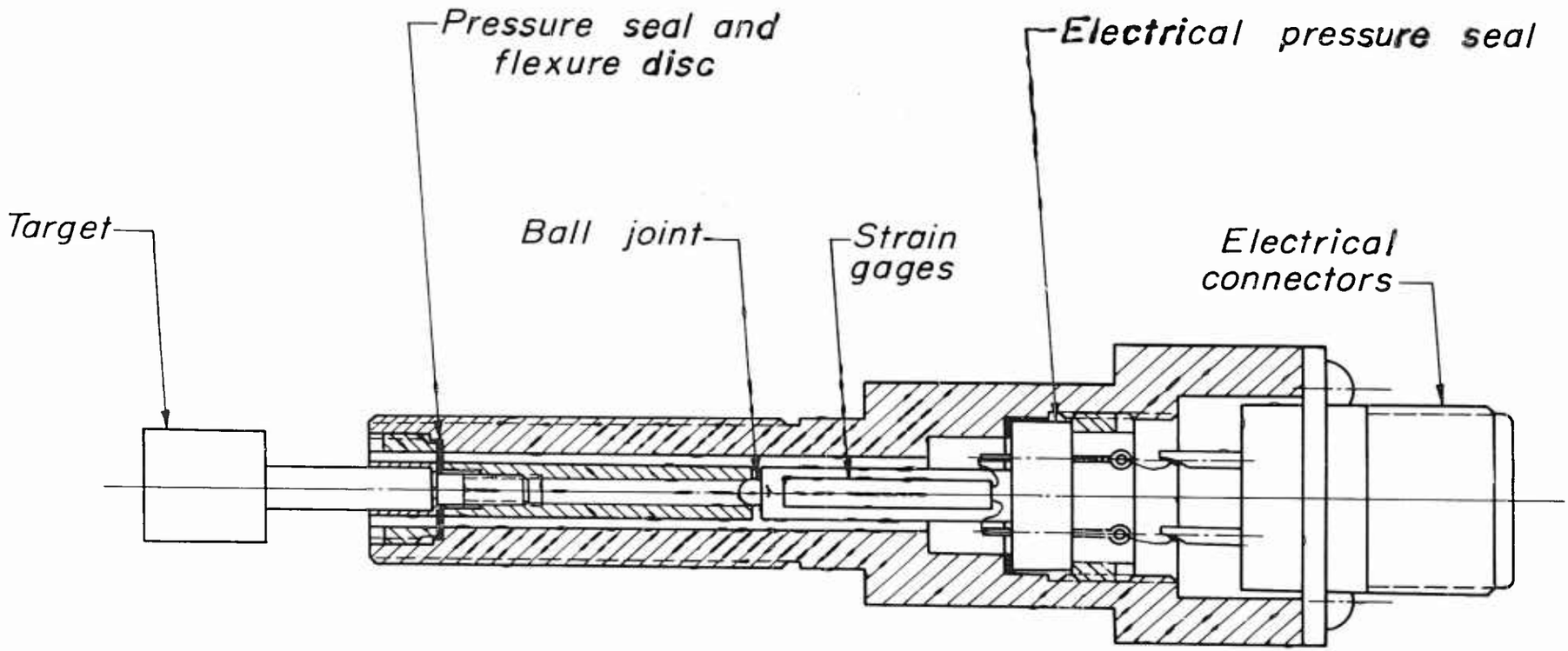

Figure 7

Detail of velocity probe

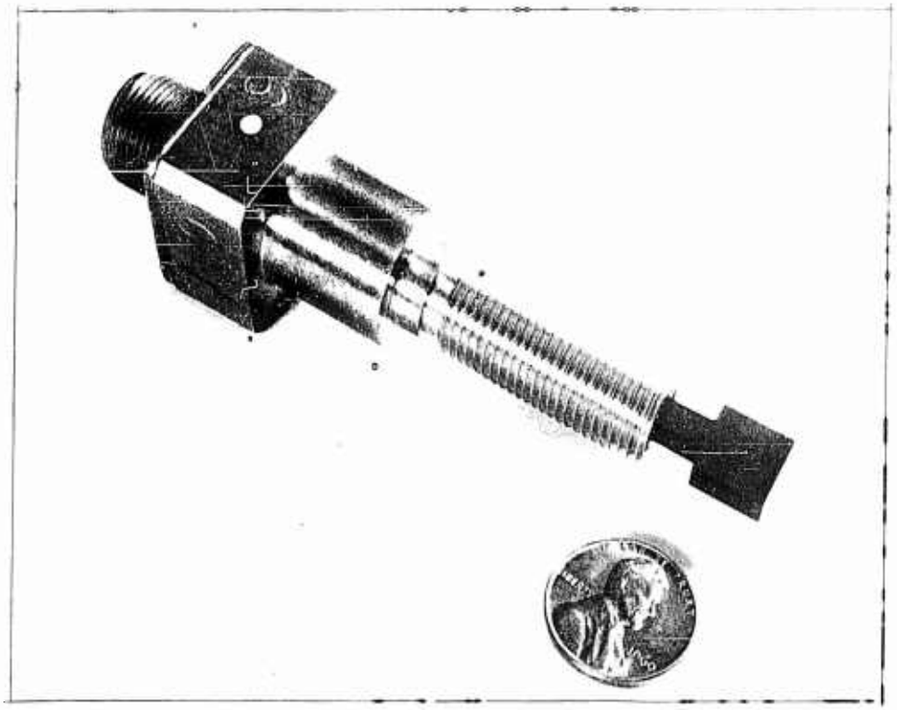

Figure 8a Velocity probe

Figure 8b Target after 2 second rocket firing ($q = 15$ BTU/in^2 sec)

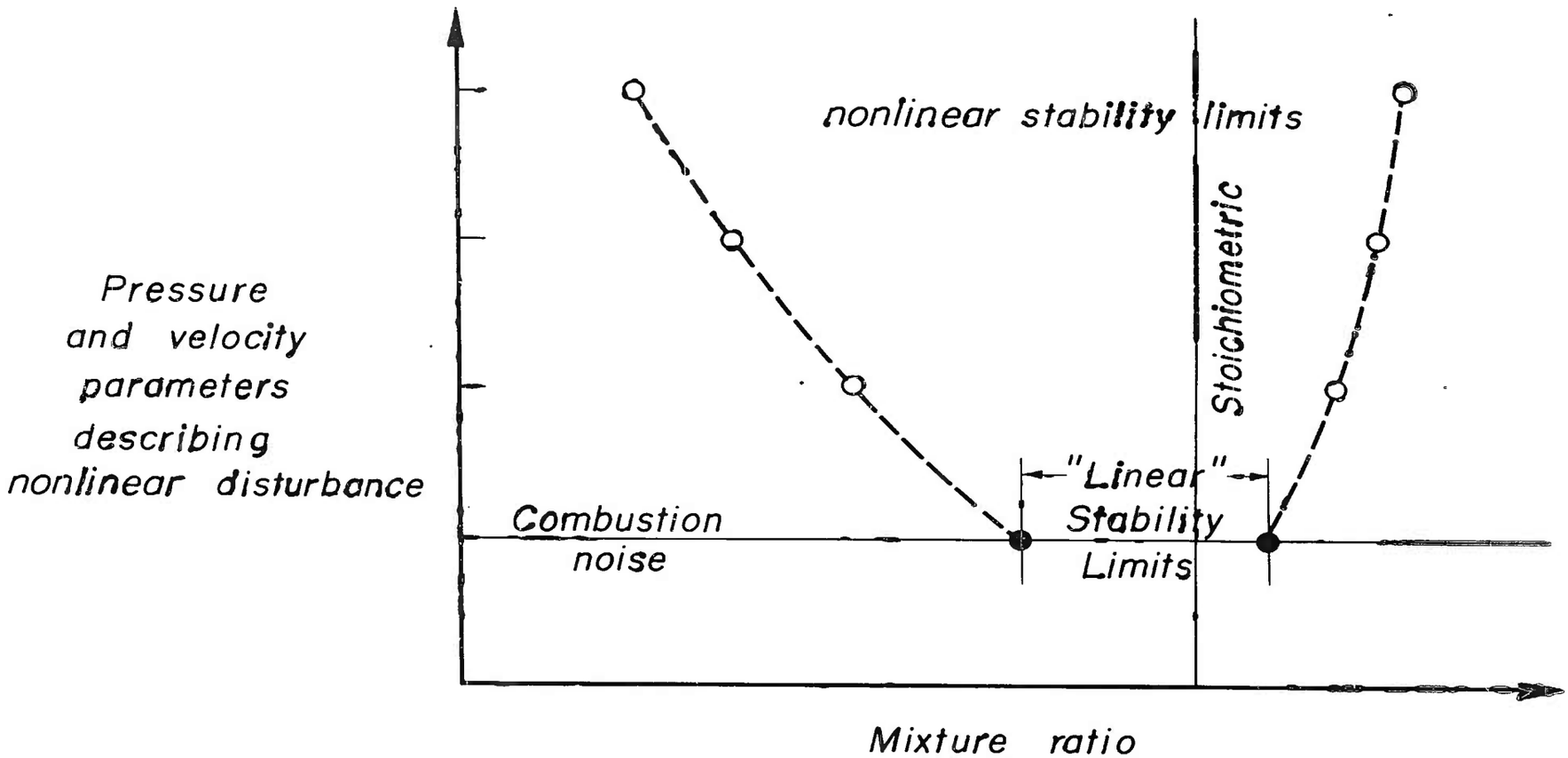

Figure 9

Schematic diagram of nonlinear stability limit tests

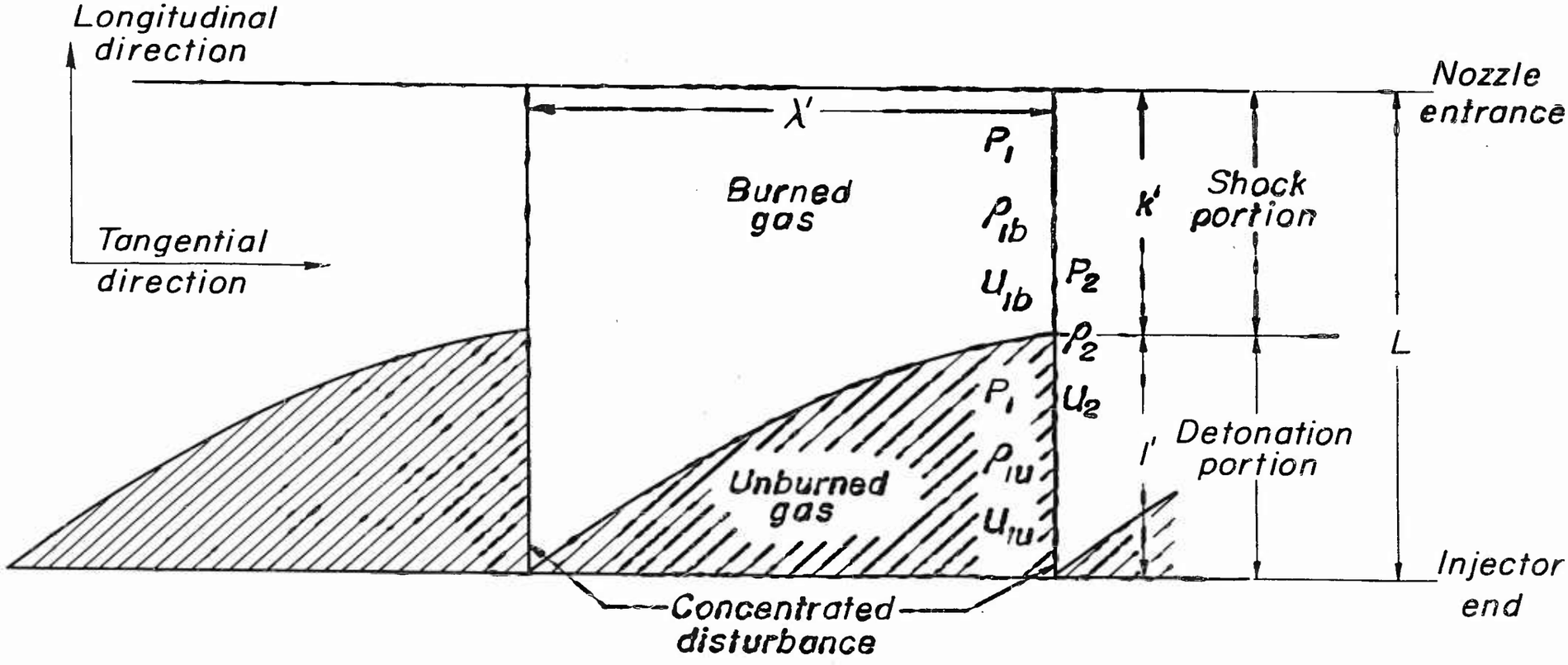

Figure 10

First nonlinear combustion instability model

DISTRIBUTION LIST

TECHNICAL AND YEARLY PROGRESS REPORTS

U. S. Dept. of the Interior
Bureau of Mines
4800 Forbes Avenue
Pittsburgh 13, Pennsylvania
Attn: M. P. Benoy, Reports Lib.
Explosive Research Lab. (1)

Central Intelligence Agency
2430 E Street, N. W.
Washington 25, D. C.
Attn: OCD, Standard Dist. (1)

NASA
1512 H Street, N. W.
Washington 25, D. C.
Attn: Chief Div. of Res. Info. (5)

NASA
Langley Research Center
Langley Field, Virginia
Attn: E. R. Gilman, Librarian (1)

NASA
Lewis Research Center
21000 Brookpark Road
Cleveland 35, Ohio
Attn: Library (1)

Commander
Air Force Flight Test Center
Edwards AFB, California
Attn: FTRDL (1)
Attn: FTRPL (1)

Office of the Director of Defense
Research and Engineering
Washington 25, D. C.
Attn: D. B. Brooks
Off. of Fuels and Lubricants (1)

Dept. of the Air Force
Headquarters USAF, DCS/D
Washington 25, D. C.
Attn: AFDRT/AS (1)

Commander
Wright Air Development Division
Wright-Patterson AFB, Ohio
Attn: WCLJC (1)

Commander
Wright Air Development Div.
Wright-Patterson AFB, Ohio
Attn: WCLTLPE (1)

Commander
Air Force Ballistic Missile Div.
Air Force Unit Post Office
Los Angeles 45, California
Attn: WDSOT (1)

Commander
Air Force Missile Dev. Center
Holloman, AFB, New Mexico
Attn: MDGRT (1)

Commander
Air Force Missile Test Center
Patrick AFB, Florida
Attn: Technical Information and
Intelligence Br. (MTGRY) (1)

Commander
AF Office of Scientific Res.
ARDC 19th and E. Capitol Sts.
Washington 25, D. C.
Attn: SRHP, Dr. M. Slawsky (1)

Commander
Air Research and Dev. Command
Andrews Air Force Base
Washington 25, D. C.
Attn: RDRR-2 (1)

ASTIA
Arlington Hall Station
Arlington 12, Virginia
Attn: TIPCR (10)

Commander
Arnold Engg. Dev. Center
Air Research and Dev. Command
Tullahoma, Tennessee
Attn: AEOIM (1)

Commanding General
Aberdeen Proving Ground
Maryland
Attn: Ballistics Res. Lab.
ORDBG-BLI (1)

Commander
Army Ballistics Missile Agcy.
Redstone Arsenal, Alabama
Attn: Tech. Documents Library
ORDAB-HT (3)

U. S. Army
Chemical Research and Dev. Labs.
Army Chemical Center, Maryland
Attn: Keith H. Jacobson
Medical Research (1)

Commanding Officer
Diamond Ord. Fuze Lab.
Washington 25, D. C.
Attn: ORDTL (012) (1)

Commanding General
Frankford Arsenal
Philadelphia 37, Pennsylvania
Attn: Mr. M. E. Levy, 1331
Research Division (1)

Commanding Officer
Office of Ord. Research
Box CM, Duke Station
Durham, North Carolina (1)

Commanding Officer
Picatinny Arsenal
Dover, New Jersey
Attn: Librarian (1)

Commander
Army Rocket and Guided Missile Agcy.
Redstone Arsenal, Alabama
Attn: Technical Library (2)

Commanding Officer
Picatinny Arsenal
Liquid Rocket Propulsion Lab.
Dover, New Jersey
Attn: Technical Library (2)
Attn: Mr. Jenkins (1)

Commanding General
White Sands Missile Range
New Mexico
Attn: Library (1)

Bureau of Naval Weapons
Dept. of the Navy
Washington 25, D. C.
Attn: RMMP-24 (3)

Bureau of Naval Weapons
Dept. of the Navy
Washington 25, D. C.
Attn: RRRSY-2 (1)

Bureau of Naval Weapons
Dept. of the Navy
Washington 25, D. C.
Attn: RMMP-4 (1)

Bureau of Naval Weapons
Dept. of the Navy
Washington 25, D. C.
Attn: ReS6 (1)

Commander
Pacific Missile Range
Point Mugu, California
Attn: Tech Library, Code 212 (2)

Commander
Naval Ordnance Lab.
White Oak
Silver Spring, Maryland
Attn: E. C. Noonan (1)

Commander (Code 753)
U. S. Naval Ord. Test Station
China Lake, California (2)

Director (Code 6180)
U. S. Naval Research Lab.
Washington 25, D. C.
Attn: H. W. Carhart (1)

Dept. of the Navy
Chief of Naval Research
Washington 25, D. C.
Attn: Propulsion Chemistry
Branch - Code 426 (1)

Commanding Officer
ONR Branch Office
1030 East Green Street
Pasadena, California (1)

Superintendent
U. S. Naval Postgraduate School
Naval Academy
Monterey, California (1)

Commanding Officer
U. S. Naval Underwater Ord. Station
Newport, Rhode Island
Attn: W. W. Bartlett (1)

Aerojet-General Corporation
P. O. Box 296
Azusa, California
Attn: M. Grenier, Librarian (1)

Aerojet-General Corporation
Sacramento Plants
P. O. Box 1947
Sacramento 9, California
Attn: R. G. Weitz
Head, Tech. Info. Off. (1)

Aeronutronic
Div. of Ford Motor Company
Ford Road
Newport Beach, California
Attn: L. H. Linder, Div. Librarian (1)

Aeroprojects, Inc.
West Chester, Pennsylvania
Attn: W. Tarpley (1)

Air Reduction Company, Inc.
Murray Hill, New Jersey
Attn: Dr. Fred Balcar (1)

American Cyanamid Company
1937 W. Main Street
Stamford, Connecticut
Attn: Dr. A. L. Peiker (1)

Armour Research Foundation
Illinois Ist. of Technology
Chicago, Illinois
Attn: M. Klein (1)

Arthur D. Little, Inc.
Acorn Park
Cambridge 40, Massachusetts
Attn: D. C. Bowersock, Jr. (1)

Atlantic Research Corporation
Edsall Road & Shirley Highway
Alexandria, Virginia (2)

Bell Aircraft Corporation
Box 1
Buffalo 5, New York
Attn: T. Reinhardt (1)

Callery Chemical Company
Callery, Pennsylvania
Attn: Document Control (1)

The Dow Chemical Company
Midland, Michigan
Attn: M. S. Auro,
Tech. Serv. and Dev. Dept.
Abbott Road Buildings (1)

Esso Research and Engg. Co.
P. O. Box 51
Linden, New Jersey
Attn: Dr. J. P. Longwell
Spec. Project Unit (1)

Texaco Experiment, Inc.
P. O. Box 1-T
Richmond 2, Virginia
Attn: Elaine Well, Library (1)

Food Machinery and Chem. Corp.
Special Projects Branch
P. O. Box 38
Buffalo 13, New York (1)

The Fulton-Irgon Corporation
P. O. Box 591
Dover, New Jersey
Attn: David Lippmann (1)

General Electric Company
Rocket Propulsion Units
Building 300
Cincinnati 15, Ohio
Attn: E. St. Clair Gantz (2)

Hughes Tool Company
Aircraft Division
Culver City, California
Attn: Dr. I. Shapiro (1)

Jet Propulsion Laboratory
4800 Oak Grove Drive
Pasadena 3, California
Attn: I. E. Newlan,
Chief Reports Group (1)

Liquid Propellant Information Agcy.
Applied Physics Laboratory
The Johns Hopkins University
Silver Spring, Maryland (3)

Marquardt Corporation
16555 Saticoy Street
Box 2013 - South Annex
Van Nuys, California (1)

Minnesota Mining & Mfg. Co.
900 Bush Avenue
St. Paul 6, Minnesota
Attn: J. W. Millin (1)

New York University
Dept. of Chemical Engg.
New York 53, New York
Attn: P. F. Winternitz (1)

Olin Mathieson Chem. Corporation
Research Library
New Haven, Connecticut
Attn: Mrs. Laura M. Kajuti (1)

Peninsular Chem-Research, Inc.
P. O. Box 3597
1207 N. W. Fifth Avenue
Gainesville, Florida
Attn: Paul Tarrant (1)

Pennsalt Chemical Corp.
P. O. Box 4388
Philadelphia 18, Pennsylvania
Attn: Dr. G. Bart-Wehrenalp (1)

Phillips Petroleum Co.
145 Chemical Laboratories Bldg.
Bartlesville, Oklahoma
Attn: Nadine G. Logan (1)

Purdue University
Lafayette, Indiana
Attn: M. J. Zucrow (1)

Reaction Motors Division
Thiokol Chemical Corporation
Denville, New Jersey
Attn: D. Mann (1)

Rocketdyne
North American Aviation, Inc.
6633 Canoga Avenue
Canoga Park, California
Attn: J. Silverman (2)

Rohm and Hass Company
Restone Arsenal
Huntsville, Alabama
Attn: Librarian (1)

Shell Development Company
Emergyville, California
Attn: R. R. Ward (1)

Space Technology Labs.
P. O. Box 95001
Airport Station
Los Angeles 45, California
Attn: M. Goldman (1)

Stauffer Chemical Company
Chauncey, New York
Attn: J. R. Gould (1)

Sundstrand Turbo
Division of Sundstrand Corp.
10445 Glenoaks Blvd.
Pacoima, California
Attn: W. Unterberg (1)

Thiokol Chemical Corporation
Redstone Division
Huntsville, Alabama
Attn: Technical Director (1)

Wyandotte Chemical Corporation
Wyandotte, Michigan
Attn: R. A. Graham
Dept. of Cont. Research (1)

Monsanto Chemical Company
Research and Engg. Division
Spec. Proj. Dept. - Chemical Lane
Everett Station, Boston 49, Mass.
Attn: K. Warren Easley (1)

Union Carbide Chemicals Company
Development Department
P. O. Box 8356
South Charleston, West Virginia
Attn: Dr. H. W. Schulz (1)

Dr. W. W. Wharton
Research Laboratory, Bldg. 4762
ARGMA
Redstone Arsenal
Huntsville, Alabama (1)

Commanding Officer
Office of Naval Research
346 Broadway
New York 13, New York
via
Office of Naval Research
Princeton, New Jersey
Attn: Julian Levy
Resident Representative (1)

Texaco, Inc.
Texaco Research Center
Beacon, New York
Attn: Technical Library (1)

United Aircraft Corporation
400 Main Street
East Hartford, Connecticut
Attn: Library (1)

Project Squid - Librarian (1)

NASA
1520 H Street, N. W.
Washington 25, D. C.
Attn: T. L. K. Smull
Code BG (10)

Princeton University
Forrestal Research Center
Princeton, New Jersey (10)